Surface Chemistry

DOI: 10.1002/anie.201002470

Direct Three-Dimensional Imaging of the Buried Interfaces between Water and Superhydrophobic Surfaces**

Chan Luo, Hua Zheng, Lei Wang, Haiping Fang, Jun Hu, Chunhai Fan, Yong Cao,* and Jian Wang**

The investigation of how water interacts with hydrophobic solids is crucial for understanding many natural and technological phenomena, such as hydrophobic collapse in protein folding,[1] the formation of hydrophobic clays,[2] and superhydrophobicity.[3] While it is generally believed that air is trapped at the interfaces between water and superhydrophobic (SH) surfaces, direct experimental evidence for the presence of air at the microscopic level is rare.[4] Herein we present an in situ, nondestructive approach to the direct 3D imaging of the buried interfaces between water droplets and superhydrophobic surfaces by confocal laser scanning microscopy (CLSM). A 10 μm thick air cushion trapped at the interface is quantitatively visualized and shown to be responsible for the ultralow-resistance fluid flow. The two intangible hydrophobic states, that is, Wenzel and Cassie states,[5] can be distinctly identified by this advanced technique. Our new approach also opens a pathway to explore complex phenomena and regulate subtle processes that occur at the liquid–vapor–solid interface for various basic research and industrial applications.

Inspired by natural examples (e.g., lotus leaves and water strider legs),[6] the design of artificial SH surfaces by fabricating rough surface microstructures and decorating the microstructured surface with chemicals of low surface free energy has become a popular research focus, since SH surfaces have found important applications in fields from aquatic devices,[6b] microfluidic transport,[7] and protective coatings,[8] to proteins and DNA analysis.[9] The superhydrophobicity of the surfaces has been explained by two major mechanisms, assuming that water exists in either Wenzel or Cassie states on hydrophobic surfaces. In the Wenzel state, water is in intimate contact with the rough surface; the contact area is dominated by the liquid–solid interface, and water droplets adhere to the solid with both large contact angles (CAs) and rolling angles (RAs).[10] In the Cassie state, the existence of the additional liquid–vapor interface means that water is partial contact with the solid, so that droplets have large CAs but small RAs.[11] Although the two mechanisms have long been proposed for the analysis of SH surfaces, it is still a matter of debate as to which state dominates in different circumstances, owing to the lack of a direct, quantitative observation method and in-depth insights into the buried interface.[4] The interface below the liquid cannot be imaged by using techniques such as SEM, TEM, and AFM,[12] while conventional 2D optical observation provides only limited and nonquantitative information that is insufficient for constructing the whole picture of the topologically complex buried interface.[13]

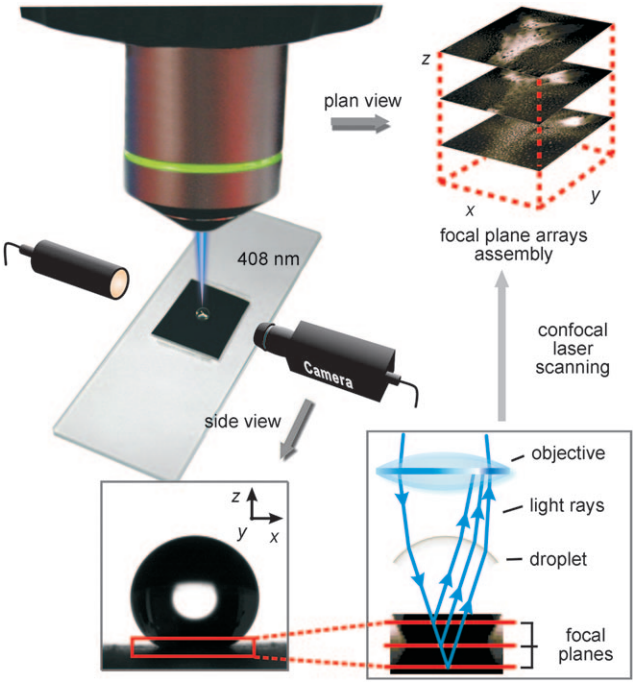

Figure 1. Side-view and the confocal laser scanning microscopy 3D plan view for observing a 10 μL water droplet on an SH sheet.

[*] Dr. C. Luo, H. Zheng, Dr. L. Wang, Prof. Y. Cao, Prof. J. Wang
Key Laboratory of Specially Functional Materials
Ministry of Education
Institute of Polymer Optoelectronic Materials and Devices
South China University of Technology
Guangzhou 510640 (P. R. China)
Fax: (+86) 20-8711-0606
E-mail: yongcao@scut.edu.cn
jianwang@scut.edu.cn
Dr. C. Luo, Prof. H. Fang, Prof. J. Hu, Prof. C. Fan
Laboratory of Physical Biology
Shanghai Institute of Applied Physics
Chinese Academy of Sciences, Shanghai 201800 (P. R. China)
E-mail: fchh@sinap.ac.cn

[**] This work was supported by the Ministry of Science and Technology of China (973 Program 2009CB623604, 2009CB930604, 2007CB936000, 2006CB93000, and 863 Program 2008AA03A311), the National Natural Science Foundation of China (20725516 and 90913014), and the China Postdoctoral Science Foundation (20100470915). We thank Jun Wang (Creative Inspection System Limited, Shenzhen Branch) for technical assistance with the CLSM setups.

Supporting information for this article is available on the WWW under http://dx.doi.org/10.1002/anie.201002470.

In this work, CLSM was employed as a top-down imaging technique (Figure 1) to investigate the 3D geometry of the interface between the liquid droplet and the SH surfaces (see the Supporting Information for detailed descriptions of the technique). Figure 2 shows the resultant 3D images of the buried interfaces on two SH samples: a lotus leaf (CA = (151 ± 2)°; Figure 2a,b), and an artificially prepared carbon nanotube/Nafion nanocomposite film (CNNF; see Ref. [13a]; CA = (156 ± 2)°; Figure 2c,d). In the interfacial images for both samples, we distinctly observe the heterogeneous characteristics of the coexistence of the liquid–solid (low-reflection dark regions) and the liquid–vapor (high-reflection bright regions) interfaces that represent the Wenzel state and the Cassie state, respectively. In addition, the invisible and trapped air can be observed in 3D at the liquid–vapor–solid interfaces by the optical reflection difference (Figure S1 in the Supporting Information).

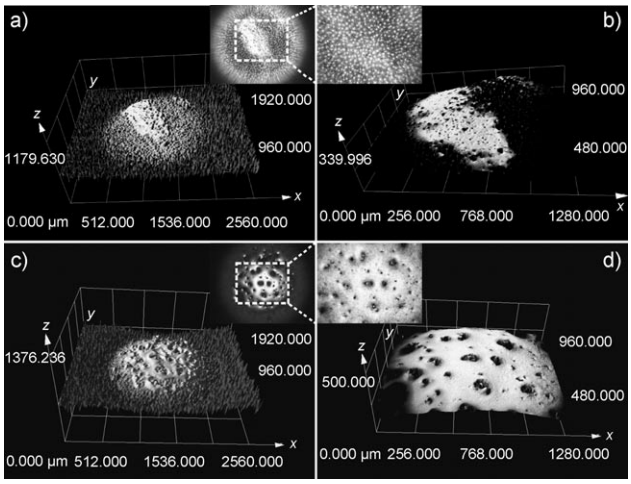

Figure 2. 3D interfacial images scanned by a 408 nm laser. a) Low- and b) high-magnification images of the lotus leaf. c) Low- and d) high-magnification images of the CNNF. The insets in (b) and (d) are the magnified images of the areas boxed by the dotted line in the insets in (a) and (c), which show the respective 2D images captured under white-light illumination.

The 3D images of the bare surfaces captured after removal of the droplet (Figure 3c,d) are different from those of the buried interfaces between the droplet and the two SH samples (Figure 3a,b), and show evenly distributed, uniform micrometer-sized papillae (inset SEM image, Figure 3c) on the lotus leaf surface, or randomly distributed, protruding nanotube aggregates of various sizes on the CNNF surface (Figure 3d, inset). The disparity between the irregular liquid–vapor–solid interface (Figure 3a) and the relatively regular topology of the lotus leaf (Figure 3c) can be attributed to the inhomogeneous distribution of hydrophobic wax because of the decay of surface chemical compositions.[6a] For the CNNF sample, large-sized aggregates on its surface (Figure 3d) penetrate into the droplet to form the liquid–solid interface (dark region, Figure 3b), whereas the remaining surface area is covered by the trapped air (bright region, Figure 3b). After addition of a fluorescent dye to the water droplet, the fluorescence confocal image gives consistent topological patterns of the liquid–vapor–solid interface (Figure S2 in the Supporting Information). Our results provide direct experimental evidence for the long-held speculation that water droplets on self-cleaning SH surfaces behave like an Indian fakir on a bed of nails.[14]

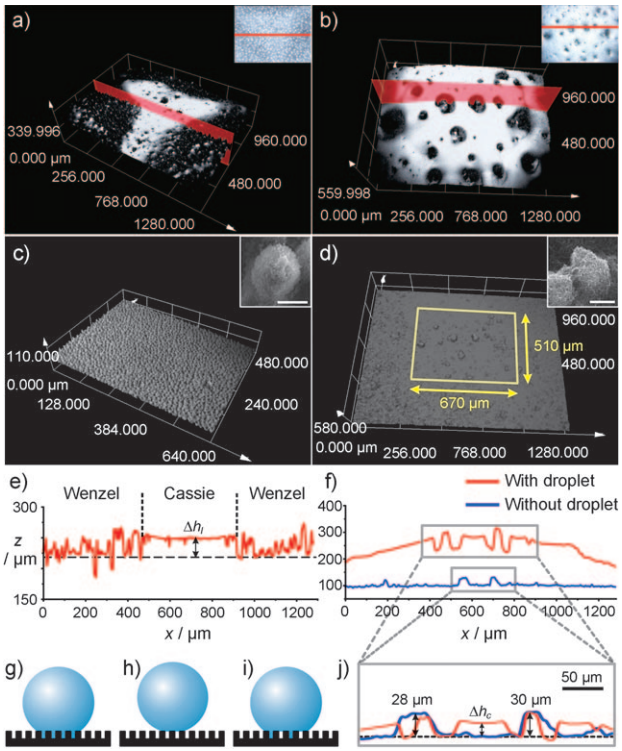

Figure 3. 3D images of the interfaces between the water droplet and the lotus leaf (a) and the CNNF (b). The insets show the respective 2D images. The red plane/line in the 3D/2D images is the probe plane/line for roughness measurements. 3D images of the bare surfaces of the lotus leaf (c) and the CNNF (d) captured after removing the droplet. The marked area of 670 µm × 510 µm in (d) corresponds to the entire area in (b). The insets show SEM images of a papilla on the lotus leaf and a nanotube aggregate on the CNNF. Scale bars = 5 µm. Respective roughness line profiles (e) and (f) measured at the intersections of interfaces with probe planes shown in (a) and (b), respectively. Schematic diagrams of the ideal Wenzel (g), Cassie (h), and the mixed Wenzel–Cassie (i) states. Determination of the thickness of the air cushion trapped between the two aggregate markers (j) by aligning the restored interface profile (red) to the bare surface profile (blue) of the CNNF sample.

We further quantitatively determined the interfacial structures through roughness measurements with CLSM, in which we used the probe plane that vertically intersects the interface along the x direction (Figure 3a,b, red planes). Both roughness tracing line profiles (Figure 3e,f, red curves) are characteristic of the mixed hydrophobic state. On the lotus leaf (Figure 3e), the roughness R_a (the arithmetic average of absolute values of the deviation from the mean of a surface profile) of the liquid–vapor interface ($470 < x < 910$ µm) is calculated to be 1.69 µm, whereas those of the liquid–solid interfaces have much larger values of 12.40 µm ($0 < x < 470$ µm) and 10.16 µm ($910 < x < 1280$ µm), thus suggesting that water infiltrates into the voids between papillae and wets the surface at the rough liquid–solid interface (see the ideal

Wenzel state, Figure 3g), while the smooth liquid–vapor interface results from the trapped air cushion that flattens the interface roughness to prevent water penetration (see the ideal Cassie state, Figure 3h). The interface profile of CNNF (red curve, Figure 3f) resembles that of the lotus leaf, except that nanotube aggregates on CNNF are lower in density but significantly broader and higher in size than papillae on the lotus leaf. Both profiles unambiguously reveal a mixed Wenzel–Cassie state at the SH surface–water interface (Figure 3i), which has recently been hypothesized.[5]

It is of great importance to measure the thickness of the air cushion trapped inside the buried interface. By taking into account the lateral magnification of 1.87 and the axial magnification of 2.63 (see the Supporting Information), the two aggregate markers in the restored interfacial profile (red curve) overlap those in the bare surface profile (blue curve; Figure 3j). The thickness of the air cushion trapped between the two aggregate markers Δh_c is therefore calculated to be approximately 16 μm. For reference, the two aggregate heights are approximately 28 μm (left) and 30 μm (right). As the lotus leaf surface lacks specific markers, the height differences between the flat liquid–vapor interface top in the middle, and the liquid–solid interface base at the two sides (Figure 3e) were used to estimate the air cushion thickness Δh_l on the lotus leaf to be approximately 10–15 μm. The estimated thickness is comparable to the actual heights of papillae measured on the leaf surface (Figure S5 in the Supporting Information), thus implying again that air fills the voids between papillae to prevent water penetration. More importantly, the existence of the 10 μm thick air cushion could possibly account for the hydrophobic interactions that occur over a very long range between two SH surfaces.[15]

It was speculated that the air cushion may dramatically reduce droplet adhesion to the SH surface, thus leading to the ultralow-resistance fluid flow (rolling rather than sliding),[16] which makes the droplets remove contaminant particles (self-cleaning). To verify this hypothesis, we designed an ultrasonic treatment to conveniently trigger the SH state transition from Cassie to Wenzel on the CNNF (see the Supporting Information). After the treatment, the water droplet that would readily roll off (RA < 5°, Figure 4a) on the CNNF now was pinned with ultrahigh affinity, like a droplet on rose petals.[17] The droplet did not fall off even when the film was turned upside down (Figure 4b). This striking difference in dynamic behavior arises from the violent movement of the water molecules. This motion was induced by the ultrasonic wave and forced evacuation of the trapped air out of the buried interface. Both 3D and 2D images of the interface consistently revealed that little air existed at the interface after the treatment, thus confirming the Cassie-to-Wenzel state transition (Figure 4c). This treated interface predictably resembles the interface between a water droplet and a smooth hydrophobic surface free of the trapped air, for example, an *n*-octadecyltrichlorosilane (OTS) coated SiO_2/Si substrate (Figure 4d). Moreover, the CA of the droplet after ultrasonic treatment is approximately 133°, which is not much different from the pre-treatment value of 155°. In comparison, the CA of the droplet on a non-air-trapped hydrophobic OTS surface is 104° (the droplet can also stick to it upside down). The

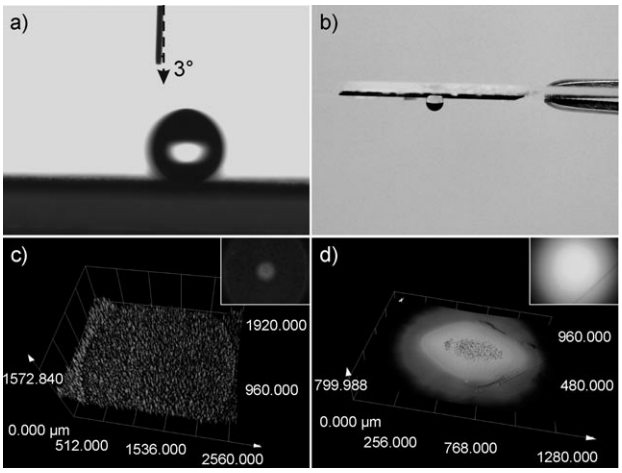

Figure 4. a) Before the ultrasonic treatment, a water droplet of 10 μL began to roll on the CNNF when the tilt angle was only 3°. The camera and sample were rotated together during the measurement, while the syringe stayed unmoved. b) Water droplet adhesion on the CNNF after ultrasonic treatment. 3D images of the interfaces between the droplet and the CNNF c) after ultrasonic treatment, and d) between the droplet and *n*-octadecyltrichlorosilane-coated SiO_2/Si substrate; the scratches on the substrate were made to help focus. The insets show the respective 2D images.

extremely mobile behavior can be largely restored (RA < 5°) after removing the droplet and drying the CNNF surface under moderate heating (60 °C for 30 min). The trapped air inside the interface is therefore responsible for not only the high CA (SH property), but also the small RA (self-cleaning property).

The dynamic transition of hydrophobic states from Cassie to Wenzel could be monitored in real time by introducing the wetting agent sodium dodecylbenzenesulfonate (SDS; 0.8 mg mL^{-1}) into the droplet. The amphiphilic surfactant molecules lower the surface tension of the water and reduce the liquid–solid interfacial tension upon absorption of the surfactant molecules by the solid surface, thereby allowing filtration of the liquid into the rough SH surface.[18] Consecutive images (Figure 5a–h) demonstrated gradual loss of the trapped air and continuous expansion of the liquid–solid interface until almost all the trapped air was released after 22 minutes (Figure 5g). The whole wetting process was also recorded using a conventional optical microscope (Movie 1 in the Supporting Information). In contrast, a control experiment with a pure water droplet deposited on the same CNNF surface showed little variation of the trapped air volume (Movie 2 in the Supporting Information). The CA of the SDS droplet immediately after the trapped air was released was 138°, which is comparable to that obtained after ultrasonic treatment. Meanwhile, the dynamical behavior again altered dramatically from an unsteady state of RA < 5° to a highly stable state that allowed exceptional adhesion of the droplet to the upside-down film, thus confirming that the trapped air is indeed responsible for the extreme mobility of the droplets.

In summary, a simple yet powerful technique that employs CLSM was used to directly observe the air trapped in the buried interface between water and SH surfaces. This 3D observation not only revealed the existence of a mixed

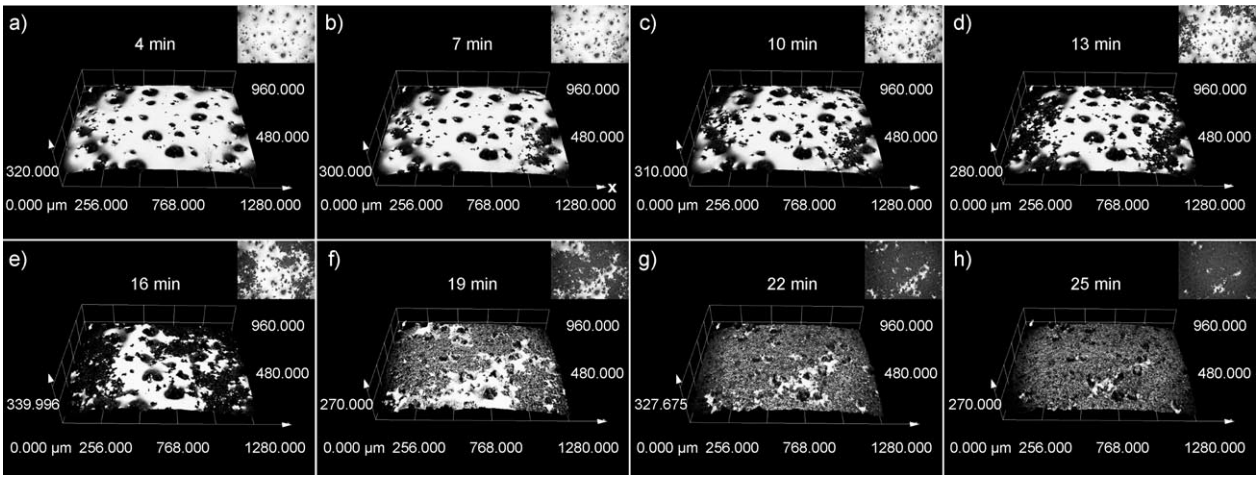

Figure 5. a–h) Consecutive 3D images of the dynamic transition from Cassie state to Wenzel state, captured with a time interval of 3 min. The insets show the respective 2D images.

Wenzel–Cassie state at the interface, but also enabled the two states to be quantitatively visualized. The presence of a 10 µm thick air cushion at the buried interface dramatically reduces water adhesion, thus resulting in self-cleaning properties of the surface. Two approaches were demonstrated to conveniently control the SH state transition from Cassie to Wenzel by either ultrasonic treatment or introduction of the surfactant SDS into the droplet, based on the knowledge acquired from the direct 3D imaging of the buried interface. Our findings will offer new mechanistic explanations to other complicated phenomena associated with interfacial water, and provide a promising approach to actively manipulate important processes such as protein folding and microfluidic transport.

Experimental Section

CNNFs containing 9 wt% Nafion were prepared by following our previously reported method.[13a] The lotus leaf was collected and transported on ice from the field to the laboratory. The OTS-coated SiO_2/Si substrate was fabricated by following the method reported by Nuckolls et al.[19] For all experiments, deionized water (Milli-Q) was used. SDS powder (purity > 95%) was purchased from Tokyo Chemical Industry. 10 µL liquid droplets (deposited from a calibrated Eppendorf micropipette) were used for all experiments unless otherwise specified. Detailed descriptions for optical studies and characterizations, CA and RA measurements, SEM, and ultrasonic treatment are provided in the Supporting Information.

Received: April 26, 2010
Revised: August 20, 2010
Published online: October 7, 2010

Keywords: hydrophobic effect · interfaces · nanotubes · superhydrophobicity · surface chemistry

[1] a) J. Israelachvili, H. Wennerstrom, *Nature* **1996**, *379*, 219–225; b) R. H. Zhou, X. H. Huang, C. J. Margulis, B. J. Berne, *Science* **2004**, *305*, 1605–1609; c) X. J. Gong, J. Y. Li, H. J. Lu, R. Z. Wan, J. C. Li, J. Hu, H. P. Fang, *Nat. Nanotechnol.* **2007**, *2*, 709–712; d) P. Ball, *Chem. Rev.* **2008**, *108*, 74–108.
[2] Z. Király, B. Veisz, A. Mastalir, G. Kofarago, *Langmuir* **2001**, *17*, 5381–5387.
[3] a) J. Genzer, K. Efimenko, *Science* **2000**, *290*, 2130–2133; b) R. Blossey, *Nat. Mater.* **2003**, *2*, 301–306.
[4] P. Ball, *Nat. Mater.* **2009**, *8*, 250–250.
[5] a) A. Lafuma, D. Quéré, *Nat. Mater.* **2003**, *2*, 457–460; b) S. Wang, L. Jiang, *Adv. Mater.* **2007**, *19*, 3423–3424.
[6] a) W. Barthlott, C. Neinhuis, *Planta* **1997**, *202*, 1–8; b) X. F. Gao, L. Jiang, *Nature* **2004**, *432*, 36–36.
[7] P. Aussillous, D. Quéré, *Nature* **2001**, *411*, 924–927.
[8] H. Y. Erbil, A. L. Demirel, Y. Avci, O. Mert, *Science* **2003**, *299*, 1377–1380.
[9] S. D. Gillmor, A. J. Thiel, T. C. Strother, L. M. Smith, M. G. Lagally, *Langmuir* **2000**, *16*, 7223–7228.
[10] R. N. Wenzel, *Ind. Eng. Chem.* **1936**, *28*, 988–994.
[11] A. B. D. Cassie, S. Baxter, *Trans. Faraday Soc.* **1944**, *40*, 546–551.
[12] a) E. Hosono, S. Fujihara, I. Honma, H. S. Zhou, *J. Am. Chem. Soc.* **2005**, *127*, 13458–13459; b) I. A. Larmour, S. E. J. Bell, G. C. Saunders, *Angew. Chem.* **2007**, *119*, 1740–1742; *Angew. Chem. Int. Ed.* **2007**, *46*, 1710–1712; c) M. Nosonovsky, B. Bhushan, *Nano Lett.* **2007**, *7*, 2633–2637; d) S. Srinivasan, V. K. Praveen, R. Philip, A. Ajayaghosh, *Angew. Chem.* **2008**, *120*, 5834–5838; *Angew. Chem. Int. Ed.* **2008**, *47*, 5750–5754; e) P. Lu, Q. Huang, B. D. Liu, Y. Bando, Y. L. Hsieh, A. K. Mukherjee, *J. Am. Chem. Soc.* **2009**, *131*, 10346–10347.
[13] a) C. Luo, X. L. Zuo, L. Wang, E. G. Wang, S. P. Song, J. Wang, C. H. Fan, Y. Cao, *Nano Lett.* **2008**, *8*, 4454–4458; b) M. S. Bobji, S. V. Kumar, A. Asthana, R. N. Govardhan, *Langmuir* **2009**, *25*, 12120–12126.
[14] a) D. Quéré, *Nat. Mater.* **2002**, *1*, 14–15; b) D. A. Doshi, P. B. Shah, S. Singh, E. D. Branson, A. P. Malanoski, E. B. Watkins, J. Majewski, F. van Swol, C. J. Brinker, *Langmuir* **2005**, *21*, 7805–7811.
[15] S. Singh, J. Houston, F. van Swol, C. J. Brinker, *Nature* **2006**, *442*, 526–526.
[16] D. Richard, D. Quéré, *Europhys. Lett.* **1999**, *48*, 286–291.
[17] J. M. Xi, L. Jiang, *Ind. Eng. Chem. Res.* **2008**, *47*, 6354–6357.
[18] K. S. Lee, N. Ivanova, V. M. Starov, N. Hilal, V. Dutschk, *Adv. Colloid Interface Sci.* **2008**, *144*, 54–65.
[19] Q. Miao, M. Lefenfeld, T. Q. Nguyen, T. Siegrist, C. Kloc, C. Nuckolls, *Adv. Mater.* **2005**, *17*, 407–412.

